

Microtearing turbulence saturation via electron temperature flattening at low-order rational surfaces

Ajay C. J.¹, Ben McMillan¹, and M. J. Pueschel^{2,3}

¹Centre for Fusion, Space and Astrophysics, Department of Physics,
University of Warwick, CV4 7AL, Coventry, UK

²Dutch Institute for Fundamental Energy Research, 5612 AJ Eindhoven, The Netherlands

³Eindhoven University of Technology, 5600 MB Eindhoven, The Netherlands

(Dated: July 20, 2022)

Microtearing instability is one of the major sources of turbulent transport in high- β tokamaks. These modes lead to very localized transport at low-order rational magnetic field lines, and we show that they can saturate by flattening the local temperature gradient. This saturation process depends crucially on the density of rational surfaces, and thus the system-size, and gives rise to a worse-than-gyro-Bohm transport scaling for system-sizes typical of existing tokamaks and simulations.

Confinement in tokamaks is enabled by magnetic field lines that trace out nested toroidal surfaces. On *rational* surfaces, the field lines connect back to themselves after integer numbers of poloidal and toroidal turns; certain electromagnetic plasma instabilities, such as the microtearing modes of interest here, are localized near these rational surfaces, and break the nested topology by forming magnetic islands [1–3]. Therefore, microtearing modes have a significant impact on confinement in high- β spherical tokamaks [4–6] and understanding microtearing transport is crucial for designing large spherical tokamak reactors such as STEP [7]. In general, gyro-Bohm [8] transport scaling may be applied when the turbulence is primarily electrostatic and allows extrapolation of predictions and observations to reactor-scale, but microtearing turbulence is less well-understood - for instance, first-principles gyrokinetic simulations often fail to saturate. We report a microtearing saturation mechanism that clarifies certain computational difficulties and provides insight into system-size scaling.

Microtearing modes are characterized by radially-narrow parallel electron current layers that are driven resonantly at the rational surface and associated magnetic islands. While various branches of microtearing modes have been identified, including those driven by the time-dependent thermal force [9] or by curvature [10, 11], and are present in various collisionality regimes [12–15], the electron temperature gradient remains a necessary condition for instability in all cases. Previous works have reported various microtearing saturation mechanisms: by background shear flow [5], zonal flows [16] or zonal fields [17]. However, despite these advances, predicting saturation levels remains a challenging task. We explore a microtearing turbulence saturation mechanism where the magnetic islands associated with the resonant current layers flatten the electron temperature gradient, thereby reducing the linear drive at the rational surfaces.

The radial width of the resonant region at the rational surfaces is generally of the order of few ion Larmor radii and is set by the parallel correlation length in linear theory which scales with the square root of the mass ratio

between ions and electrons [18]. Nonlinearly, the flux associated with these modes, although slightly broadened, is still localized at the rational surfaces. This is already known to be important in setting global flux levels in the pedestal [19]. In the most extreme case, if turbulent diffusivity is sufficiently large and localized near low-order rational surfaces, the system will remove the local driving gradients, increase the gradients away from the low-order rational surfaces, and saturate in a zero-flux state. In this work, we find a less extreme version of this process occurring in a standard microtearing regime. We make a scaling argument to quantify this effect and suggest that future reactor-size devices subject to microtearing turbulence may perform worse than expected.

We proceed by demonstrating the strong electron-temperature-gradient flattening at low-order rationals in gyrokinetic simulations, and showing that this allows saturation by reducing mode drive. We test the impact of the various saturation mechanisms by suppressing zonal modulations and show the dominance of the temperature corrugations. Lastly, we consider system-size scaling and explain the origin of a non-gyro-Bohm scaling.

Simulation set-up.—Our numerical investigation uses GENE flux-tube gyrokinetic simulations [20] with a field-aligned coordinate system [21] where x is the radial coordinate, y the binormal coordinate and z the parallel coordinate. The physical and numerical parameters used in this study are taken from Ref. [22]. Concentric circular flux-surface geometry [23] is considered with an inverse aspect ratio $\epsilon = 0.18$, safety factor $q_0 = 3$, magnetic shear $\hat{s} = 1$, mass ratio $m_i/m_e = 1836$, temperature ratio $T_{i,0}/T_{e,0} = 1$ and normalized pressure $\beta = 0.4\%$. The inverse of the density, ion temperature and electron temperature background gradient scale lengths, normalized to the major radius R , are $R/L_n = 1$, $R/L_i = 0$ and $R/L_e = 4.5$, respectively. To model collisions, the linearised Landau operator is used with an electron-ion collision frequency $\nu_{ei}/(v_{th,e}/R) = 0.02$, where $v_{th,s} = (T_{s,0}/m_s)^{1/2}$ is the thermal velocity of species s .

The standard nonlinear simulation considered in

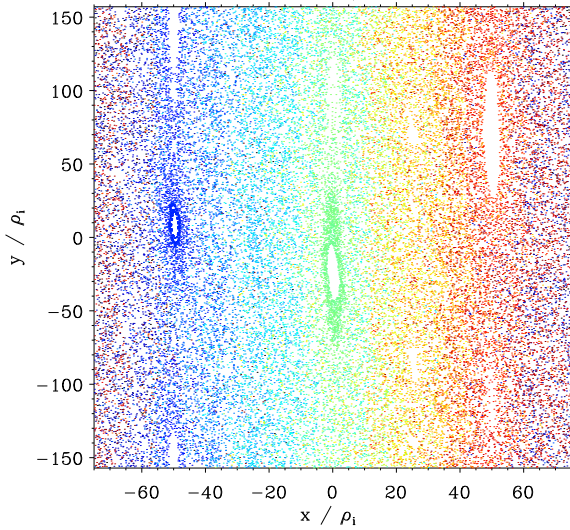


FIG. 1. Poincaré plot of magnetic field lines intersecting the outboard midplane for the standard nonlinear simulation at $tv_{th,i}/R = 1750$.

this work, with a minimum binormal wavenumber of $k_{y,\min}\rho_i = 0.02$ and run until normalized time $tv_{th,i}/R = 2000$, saturates to give a gyro-Bohm normalized electron electromagnetic heat flux of $Q_{e,em}/Q_{GB} = 7.9$ (see Fig. 5). The corresponding k_y spectrum of $Q_{e,em}$ peaks at $k_y\rho_i = 0.04$.

T_e flattening at low-order rational surfaces.—Modes at a specific toroidal mode number k_y create magnetic islands around the resonantly driven current layers at their respective mode rational surfaces (MRSs). Note that the distance between MRSs for a given k_y is $1/(sk_y)$. The MRS of all k_y radially align at the lowest-order mode rational surface (LMRS), where the magnetic islands can persist even in the turbulent phase. For the standard nonlinear simulation, this can be seen at the LMRSs at $x/\rho_i = -50, 0$ and 50 in the Poincaré plot in Fig. 1. The Poincaré plot records the positions where each magnetic field line crosses the outboard midplane on successive poloidal turns [24, 25]. Each color denotes an individual field line. Away from the LMRSs, the MRSs of each k_y are radially misaligned and the overlapping magnetic islands give rise to ergodic regions.

As the electrons move swiftly along the parallel direction following the perturbed magnetic field associated with the islands at the low-order MRSs, they also undergo periodic radial excursions. This leads to a short-circuit of the perturbed T_e profile, leading to its flattening. This can be seen in Fig. 2, where the green curve denoting the time-averaged effective temperature gradient $\omega_{T_e}^{\text{eff}}$ is plotted as a function of the radial coordinate for the standard nonlinear simulation. $\omega_{T_e}^{\text{eff}}$ is defined as the sum of the contributions from the background temperature gradient and the time-averaged zonal per-

turbed temperature gradient, *i.e.* $\omega_{T_e}^{\text{eff}} = R/L_{T_e} - \langle \partial \delta T_e / \partial x \rangle_{yz} / (T_{0,e}/R)$. The flux-surface average, denoted by $\langle \cdot \rangle_{yz}$, extracts the zonal contribution. This temperature flattening is a microturbulence analogue of profile flattening resulting from the large-scale neoclassical tearing modes (NTMs).

One can also understand the temperature flattening as a consequence of the turbulence self-interaction - a mechanism where modes that are significantly extended along the field line ‘bite their tails’ at the rational surfaces [26, 27]. In the case of microtearing modes, the parallel electron heat current density $q_{e,\parallel} = \int v_{\parallel}^3 \delta f_e d^3 v$ which is extended along the field line, interacts with the A_{\parallel} of the same eigenmode, to drive zonal parallel electron temperature perturbations $\langle \delta T_{e,\parallel} \rangle_{yz}$, leading to its flattening at MRSs. Here, δf_e is the perturbed electron distribution function and $\delta T_{e,\parallel} = (m_e/n_0) \int v_{\parallel}^2 \delta f_e d^3 v$.

Taking the v_{\parallel}^2 moment and the flux-surface average of the gyrokinetic Vlasov equation, one arrives at an equation for the time evolution of the zonal $\delta T_{e,\parallel}$. Considering only the electromagnetic ($\propto A_{\parallel}$) nonlinear term and ignoring the gyro-average over A_{\parallel} , one obtains

$$\frac{\partial \langle \delta T_{e,\parallel} \rangle_y}{\partial t} \approx - \frac{m_e}{n_0} \frac{1}{\mathcal{C}} \frac{\partial}{\partial x} \sum_{k_y} i k_y \hat{q}_{e,\parallel,k_y} \hat{A}_{\parallel,k_y}^*$$

where the constant $\mathcal{C} = B_0 / |\nabla x \times \nabla y|$. The linear structures of $\hat{q}_{e,\parallel,k_y}$ and \hat{A}_{\parallel,k_y} for $k_y\rho_i = 0.04$ are plotted with dashed lines in Fig. 3. The product of the two, proportional to a linear heat flux contribution, drives a zonal $\delta T_{e,\parallel}$ that leads to the flattening of the parallel electron temperature at each MRS. The same process repeats for the perpendicular electron temperature.

However, note a significant broadening of the time-averaged $\hat{q}_{e,\parallel,k_y}$ in nonlinear simulation, also shown in

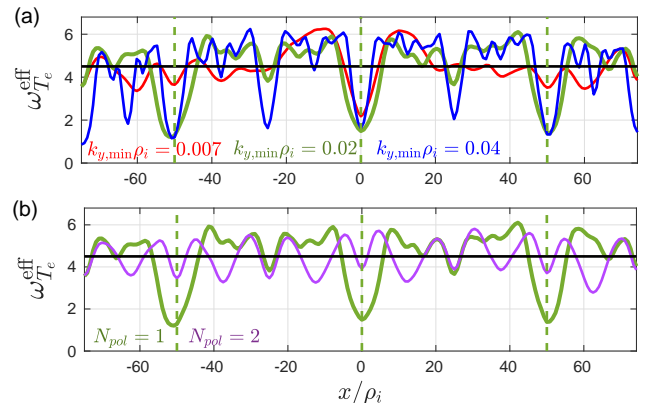


FIG. 2. (a) Time-averaged $\omega_{T_e}^{\text{eff}}$ in simulations with $k_{y,\min}\rho_i = 0.007$ (red), $k_{y,\min}\rho_i = 0.02$ (green) and $k_{y,\min}\rho_i = 0.04$ (blue). (b) Time-averaged $\omega_{T_e}^{\text{eff}}$ in simulations with $N_{pol} = 1$ (green) and $N_{pol} = 2$ (violet). Black horizontal lines indicate $R/L_{T_e} = 4.5$. Green vertical dashed lines indicate LMRSs for $k_{y,\min}\rho_i = 0.02$.

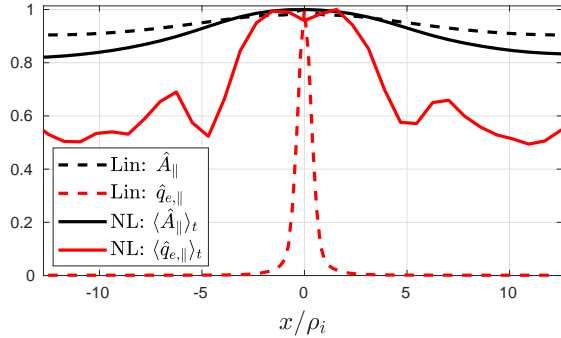


FIG. 3. Parallel vector potential \hat{A}_{\parallel,k_y} (black) and parallel electron heat current $\hat{q}_{e,\parallel}$ (red) for the microtearing mode with $k_y\rho_i = 0.04$. The linear eigenmode is shown in dashed lines and the time-averaged nonlinear data in solid lines, all normalized by their maximum.

Fig. 3 with a solid red line. A detailed description of this nonlinear broadening mechanism is given in Refs. [27, 28] and can be summarized as follows. The radially narrow linear eigenmode structures lead to extended tails in k_x -Fourier space and in ballooning representation (called ‘giant tails’ [29]). However, in a nonlinear simulation, only the first few linearly coupled k_x -Fourier modes starting from $k_x = 0$ of the eigenmode are able to retain their linear characteristics, *i.e.*, their high amplitudes and relative phase differences with the $k_x = 0$ mode, whereas the Fourier modes further away in the tail undergo a significant reduction in their amplitudes as a result of dominant nonlinear interactions, implying a broadening in real space. The width of the flattened electron temperature is therefore also broadened.

Microtearing stability with corrugated background gradients.—Now, we consider the linear stability of microtearing modes when the effective electron temperature gradient $\omega_{T_e}^{\text{eff}}$ has local flattenings at LMRSs; the profiles are plotted in Fig. 4(a). This is equivalent to the tertiary instability analysis of zonal flows [30], except with a fixed temperature corrugation rather than a zonal flow pattern.

Since the resonant current drive leading to the microtearing instability is also localized at the MRS, we expect the growth rate of the $k_y\rho_i = 0.02$ modes considered in these tertiary instability simulations to be set mostly by the effective gradient $\omega_{T_e,\text{MRS}}^{\text{eff}}$ at the MRS, *i.e.*, the temperature gradient away from MRS is of little significance. This is verified in Fig. 4(b) by the close match between the growth rate obtained from the tertiary instability simulations plotted as a function of $\omega_{T_e,\text{MRS}}^{\text{eff}}$ (magenta) and the growth rate obtained from standard linear simulations plotted as a function of R/L_{T_e} (blue). The figure also suggests that the time averaged $\omega_{T_e,\text{MRS}}^{\text{eff}}$ in standard nonlinear simulation is set by the critical gradient of the instability. That is, the system may saturate

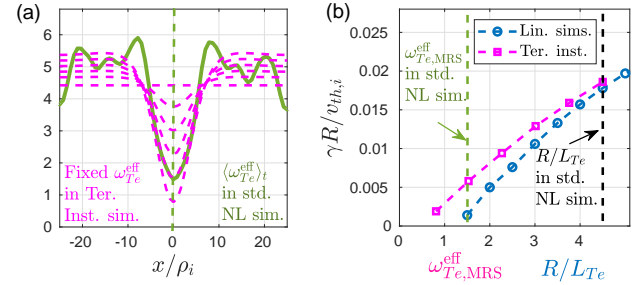


FIG. 4. (a) Magenta: Various fixed $\omega_{T_e}^{\text{eff}}$ considered for the tertiary instability simulations. Solid green: Time-averaged $\omega_{T_e}^{\text{eff}}$ in the standard nonlinear simulation. Dashed green: Position of the MRS. (b) Magenta: Growth rate in tertiary instability simulations as a function of $\omega_{T_e,\text{MRS}}^{\text{eff}}$. Blue: Growth rate in linear simulations as a function of R/L_{T_e} .

by reducing the local drive of microtearing modes, almost stabilizing them in this case.

Removing zonal modulations.—To further investigate the role of electron temperature flattening on saturation, a nonlinear simulation is run while eliminating any local modifications to the temperature gradient. This is achieved by redefining the zonal component of the electron distribution function as $\langle \delta f_e \rangle_{yz} = \langle \delta f_e \rangle_{yz} - K[v^2 - 1.5]\langle f_M \rangle_{yz}$. At each time-step, K is set such that $\langle \delta T_e \rangle_{yz} = 0$, so that $\omega_{T_e}^{\text{eff}} = R/L_{T_e}$ throughout the simulation. The heat flux $Q_{e,\text{em}}/Q_{GB} = 28.1$ in this simulation is many times higher than $Q_{e,\text{em}}/Q_{GB} = 7.9$ in the original standard nonlinear simulation, as shown in Fig. 5, confirming that electron temperature flattening indeed plays a significant role in saturation.

Another way to reduce the electron temperature flattening is by weakening the self-interaction process by increasing the parallel length $L_z = 2\pi N_{pol}$ of the simulation volume [26, 27, 31], where N_{pol} indicates the number of times the flux-tube wraps around poloidally before connecting back to itself. Increasing N_{pol} weakens the temperature flattening, as shown in Fig. 2(b), and increases the flux level as shown in Fig. 5.

While these results confirm that the local flattening of electron temperature is crucial for correctly predicting the saturated turbulent state, the fact that these simulations, either with fully eliminated or weakened electron temperature flattenings, did saturate, indicates the presence of other saturation mechanism(s). Deleting the zonal electrostatic potential Φ or the zonal A_{\parallel} in simulations changes the flux levels at most by 12%, implying that zonal flows and fields do not play a significant role in the saturation in the case considered. Although it is unknown at the moment what the other saturation mechanism(s) is, the free-energy analysis in Ref. [32] may provide a starting point.

Effect of system-size.—Given that microtearing turbulence saturation via temperature flattening happens pri-

marily at LMRSSs, the separation distance $1/(\hat{s}k_{y,\min})$ between the LMRSSs is crucial, and we thus scan $k_{y,\min} = 2\pi/L_y$. Capturing the full toroidal domain requires $k_{y,\min}\rho_i = q_0(a/r_0)\rho^*$, where a is the minor radius and r_0 is the radial position of the flux-tube, and therefore scanning $k_{y,\min}\rho_i$ can also be interpreted as a scan in tokamak size measured by $\rho^* = \rho_i/a$ [26, 27]. For a typical MAST equilibrium [4] with $q_0 = 1.35$ at $r_0 = 0.31\text{m}$, $k_{y,\min}\rho_i \simeq 0.03$.

As $k_{y,\min}$ is decreased, the radial density of regions with flattened electron temperature (see Fig. 2(a)), and hence weaker linear drive, at low-order MRSs decreases. Concurrently, flux increases, as shown by the blue asterisks in Fig. 5. That is, the temperature flattening mechanism becomes less effective in large systems. For the $k_{y,\min}\rho_i = 0.02$ case, the $k_y\rho_i = 0.04$ mode contributing most to the flux has six MRSs, three of which at LMRSSs experience $\sim 70\%$ flattening, and the other three at second-order MRSs experience $\sim 10\%$ flattening. Whereas for $k_{y,\min}\rho_i = 0.04$, the $k_y\rho_i = 0.04$ mode sees a $\sim 70\%$ temperature flattening at every MRS, so mode stabilization is much more effective. When the electron temperature flattenings are eliminated, there is still some non-gyro-Bohm scaling (black markers in Fig. 5), but this is less consistent.

We suggest a crude model to understand the increase in flux with increasing system-size. In the turbulent steady state, when the electron heat flux Q_e becomes radially constant, one defines the pointwise diffusivity via $\chi_e \equiv Q_e/(dT_e/dx)$ and the radial average

$$\left\langle \frac{dT_e}{dx} \right\rangle_x = \left\langle \frac{Q_e}{\chi_e} \right\rangle_x = Q_e \left\langle \frac{1}{\chi_e} \right\rangle_x.$$

Boundary conditions impose zero average temperature fluctuation, thus $Q_e = dT_{e,0}/dx \langle 1/\chi_e \rangle_x^{-1}$, where $\langle 1/\chi_e \rangle_x^{-1}$ is the effective average diffusivity. Microtearing modes are modelled to lead to regions of high diffusivity near each MRS, which reinforce at LMRSSs, resulting in the temperature-gradient corrugations seen in simulations.

As the harmonic mean of diffusivity sets flux levels, concentrating the diffusivity at widely-spaced MRSs (large $k_{y,\min}$, small system-size) leads to lower flux than distributing it more evenly at a larger number of closely-spaced MRSs (low $k_{y,\min}$, large system-size). In an extreme limit, microtearing creates infinite local diffusivity and completely flattens gradients near each MRS, but elsewhere the diffusivity is a small constant χ_b . The effective average diffusivity, crudely assuming no overlap between flattened regions, is $\chi_b/(1 - WN)$, where W is the proportion of the radius flattened by each toroidal mode and N is the number of toroidal modes. This leads to a scaling $Q_e \propto 1/(1 - w/\rho^*)$ with w a small parameter; note that the flux rises sharply at small ρ^* . This is analogous to the avalanche transport arising when trans-

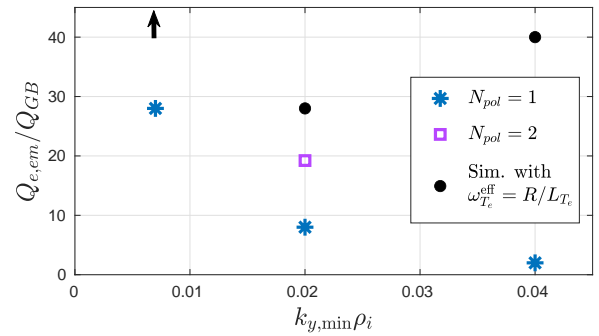


FIG. 5. Time averaged electron electromagnetic heat flux $Q_{e,em}/Q_{GB}$ as a function of $k_{y,\min}\rho_i$ in simulations with $N_{pol} = 1$ (blue asterisks) and $N_{pol} = 2$ (violet squares). Black markers indicate simulations whose electron temperature flattenings are eliminated such that $\omega_{T_e}^{eff} = R/L_{T_e}$. Up-arrow indicates that the simulation saturates only transiently.

port windows caused by fast-particle-driven modes overlap across much of the tokamak [33].

The width W of the high-transport region was assumed fixed in this simple picture, but actually may increase with higher flux, and the larger overlap may cause a runaway situation; this may be tied to failure to reach saturation in certain microtearing simulations.

Apart from system-size scaling, another possible consequence of electron temperature flattenings and magnetic islands at low-order rational surfaces is the potential to seed the growth of NTMs [34]. The possibility for microturbulence to excite NTMs via nonlinear coupling has been demonstrated in the past [35]. Furthermore, to experimentally verify our results, one may measure the electron temperature and look for flattenings near rational surfaces, similar to previous investigations of ITG turbulence [36]. One may also be able to measure low toroidal mode number magnetic perturbations associated with the microtearing islands in external magnetic coils; for instance, the radial magnetic perturbation associated with the islands is $(\delta B_x/B_0)/(\rho_i/R) \simeq 0.14$ in the standard nonlinear simulation.

In conclusion, the fast motion of electrons across the magnetic islands at the LMRSSs short-circuit the electron temperature, resulting in local electron temperature flattening, which then decreases the local linear drive of microtearing modes and allows lower saturated transport levels. The spacing and width of the low-confinement regions near low-order rationals are crucial, and this provides a pathway to understand microtearing saturation (or lack thereof); one direct consequence is that microtearing turbulent transport and its study are more important in larger future devices than previously thought.

We acknowledge the CINECA award under the ISCRA initiative, for the availability of high performance computing resources and support.

[1] R. D. Hazeltine, D. Dobrott, and T. S. Wang. Kinetic theory of tearing instability. *The Phys. Fluids*, 18(12):1778–1786, 1975.

[2] J. F. Drake, N. T. Gladd, C. S. Liu, and C. L. Chang. Microtearing modes and anomalous transport in tokamaks. *Phys. Rev. Lett.*, 44:994–997, Apr 1980.

[3] J. W. Connor, S. C. Cowley, and R. J. Hastie. Microtearing stability in tokamaks. *Plasma Phys. Controlled Fusion*, 32(10):799–817, oct 1990.

[4] D. J. Applegate, C. M. Roach, S. C. Cowley, W. D. Dorland, N. Joiner, R. J. Akers, N. J. Conway, A. R. Field, A. Patel, M. Valovic, and M. J. Walsh. Microstability in a MAST-like high confinement mode spherical tokamak equilibrium. *Phys. Plasmas*, 11(11):5085–5094, 2004.

[5] W. Guttenfelder, J. Candy, S. M. Kaye, W. M. Nevins, E. Wang, R. E. Bell, G. W. Hammett, B. P. LeBlanc, D. R. Mikkelsen, and H. Yuh. Electromagnetic transport from microtearing mode turbulence. *Phys. Rev. Lett.*, 106:155004, Apr 2011.

[6] B.S. Patel, D. Dickinson, C.M. Roach, and H.R. Wilson. Linear gyrokinetic stability of a high beta non-inductive spherical tokamak. *Nucl. Fusion*, 62(1):016009, dec 2021.

[7] H. Wilson, I. Chapman, T. Denton, W. Morris, B. Patel, G. Voss, C. Waldon, and the STEP Team. STEP-on the pathway to fusion commercialization. In *Commercialising Fusion Energy*, 2053–2563, pages 8–1 to 8–18. IOP Publishing, 2020.

[8] R. E. Waltz, J. C. DeBoo, and M. N. Rosenbluth. Magnetic-field scaling of dimensionally similar tokamak discharges. *Phys. Rev. Lett.*, 65:2390–2393, Nov 1990.

[9] J. F. Drake and A. B. Hassam. Collisional drift waves in a plasma with electron temperature inhomogeneity. *Phys. Fluids*, 24(7):1262–1269, 1981.

[10] D. Carmody, M. J. Pueschel, and P. W. Terry. Gyrokinetic studies of microinstabilities in the reversed field pinch. *Phys. Plasmas*, 20(5):052110, 2013.

[11] M. Hamed, M. Muraglia, Y. Camenen, X. Garbet, and O. Agullo. Impact of electric potential and magnetic drift on microtearing modes stability. *Phys. Plasmas*, 26(9):092506, 2019.

[12] J. F. Drake and Y. C. Lee. Kinetic theory of tearing instabilities. *Phys. Fluids*, 20(8):1341–1353, 1977.

[13] N. T. Gladd, J. F. Drake, C. L. Chang, and C. S. Liu. Electron temperature gradient driven microtearing mode. *Phys. Fluids*, 23(6):1182–1192, 1980.

[14] I. Predebon and F. Sattin. On the linear stability of collisionless microtearing modes. *Phys. Plasmas*, 20(4):040701, 2013.

[15] A. K. Swamy, R. Ganesh, S. Brunner, J. Vaclavik, and L. Villard. Collisionless microtearing modes in hot tokamaks: Effect of trapped electrons. *Phys. Plasmas*, 22(7):072512, 2015.

[16] S. Maeyama, T.-H. Watanabe, and A. Ishizawa. Suppression of ion-scale microtearing modes by electron-scale turbulence via cross-scale nonlinear interactions in tokamak plasmas. *Phys. Rev. Lett.*, 119:195002, Nov 2017.

[17] M. J. Pueschel, D. R. Hatch, M. Kotschenreuther, A. Ishizawa, and G. Merlo. Multi-scale interactions of microtearing turbulence in the tokamak pedestal. *Nucl. Fusion*, 60(12):124005, 2020.

[18] M. R. Hardman, F. I. Parra, C. Chong, T. Adkins, M. S. Anastopoulos-Tzanis, M. Barnes, D. Dickinson, J. F. Parisi, and H. Wilson. Extended electron tails in electrostatic microinstabilities and the nonadiabatic response of passing electrons. *Plasma Phys. Controlled Fusion*, 64(5):055004, 2022.

[19] D. R. Hatch, M. Kotschenreuther, S. M. Mahajan, M. J. Pueschel, C. Michoski, G. Merlo, E. Hassan, A. R. Field, L. Frassinetti, C. Giroud, J.C. Hillesheim, C.F. Maggi, C. Perez von Thun, C.M. Roach, S. Saarelma, D. Jarema, F. Jenko, and JET Contributors. Microtearing modes as the source of magnetic fluctuations in the JET pedestal. *Nucl. Fusion*, 61(3):036015, 2021.

[20] F. Jenko, W. Dorland, M. Kotschenreuther, and B. N. Rogers. Electron temperature gradient driven turbulence. *Phys. Plasmas*, 7(5):1904–1910, 2000.

[21] M. A. Beer, S. C. Cowley, and G. W. Hammett. Field-aligned coordinates for nonlinear simulations of tokamak turbulence. *Phys. Plasmas*, 2(7):2687–2700, 1995.

[22] T. Xie, M. J. Pueschel, and D. R. Hatch. Quasilinear modeling of heat flux from microtearing turbulence. *Phys. Plasmas*, 27(8):082306, 2020.

[23] X. Lapillonne, S. Brunner, T. Dannert, S. Jolliet, A. Marinoni, L. Villard, T. Görler, F. Jenko, and F. Merz. Clarifications to the limitations of the s-alpha equilibrium model for gyrokinetic computations of turbulence. *Phys. Plasmas*, 16(3):032308, 2009.

[24] W. M. Nevins, E. Wang, and J. Candy. Magnetic stochasticity in gyrokinetic simulations of plasma microturbulence. *Phys. Rev. Lett.*, 106:065003, Feb 2011.

[25] M. J. Pueschel, D. R. Hatch, T. Görler, W. M. Nevins, F. Jenko, P. W. Terry, and D. Told. Properties of high-beta microturbulence and the non-zonal transition. *Phys. Plasmas*, 20(10):102301, 2013.

[26] J. Ball, S. Brunner, and Ajay C. J. Eliminating turbulent self-interaction through the parallel boundary condition in local gyrokinetic simulations. *J. Plasma Phys.*, 86(2):905860207, 2020.

[27] Ajay C. J., S. Brunner, B. McMillan, J. Ball, J. Dominiski, and G. Merlo. How eigenmode self-interaction affects zonal flows and convergence of tokamak core turbulence with toroidal system size. *J. Plasma Phys.*, 86(5):905860504, 2020.

[28] Ajay C. J., S. Brunner, and J. Ball. Effect of collisions on non-adiabatic electron dynamics in ITG-driven microturbulence. *Phys. Plasmas*, 28(9):092303, 2021.

[29] K. Hallatschek and W. Dorland. Giant electron tails and passing electron pinch effects in tokamak-core turbulence. *Phys. Rev. Lett.*, 95:055002, Jul 2005.

[30] M. J. Pueschel, T. Görler, F. Jenko, D. R. Hatch, and A. J. Cianciara. On secondary and tertiary instability in electromagnetic plasma microturbulence. *Phys. Plasmas*, 20(10):102308, 2013.

[31] A. Ishizawa, T.-H. Watanabe, H. Sugama, S. Maeyama, and N. Nakajima. Electromagnetic gyrokinetic turbulence in finite-beta helical plasmas. *Phys. Plasmas*, 21(5):055905, 2014.

[32] H. Doerk, F. Jenko, M. J. Pueschel, and D. R. Hatch. Gyrokinetic microtearing turbulence. *Phys. Rev. Lett.*, 106:155003, Apr 2011.

[33] E. D. Fredrickson, N. N. Gorelenkov, R. E. Bell, J. E. Menard, A. L. Roquemore, S. Kubota, N. A. Crocker, and W. Peebles. Fast ion loss in a ‘sea-of-TAE’. *Nucl. Fusion*, 46(10):S926–S932, 2006.

[34] R. J. Buttery, S. Günter, G. Giruzzi, T. C. Hender,

D. Howell, G. Huysmans, R. J. La Haye, M. Maraschek, H. Reimerdes, O. Sauter, C. D. Warrick, H. R. Wilson, and H. Zohm. Neoclassical tearing modes. *Plasma Phys. Controlled Fusion*, 42(12B):B61–B73, 2000.

[35] M. Muraglia, O. Agullo, S. Benkadda, M. Yagi, X. Garbet, and A. Sen. Generation and amplification of magnetic islands by drift interchange turbulence. *Phys. Rev. Lett.*, 107:095003, Aug 2011.

[36] R. E. Waltz, M. E. Austin, K. H. Burrell, and J. Candy. Gyrokinetic simulations of off-axis minimum-q profile corrugations. *Phys. Plasmas*, 13(5):052301, 2006.